ChemComm

The Evolution of Size, Shape, and Surface Morphology of Gold Nanorods

SCHOLARONE™
Manuscripts

ChemComm

COMMUNICATION

The Evolution of Size, Shape, and Surface Morphology of Gold Nanorods

Wenming Tong[a], Hadas Katz-Boon[b], Michael J. Walsh[b], Matthew Weyland[b,c], Joanne Etheridge[b,c], Alison M. Funston[*,a]

We investigate the transformation of single crystal gold nanorod surface morphology over extended growth times. After initial rapid anisotropic growth and disappearance of {111} bridging facets, the aspect ratios converge across AgNO$_3$ concentrations. The surface morphology transitions from faceted to curved. These observations imply the final aspect ratio has little dependence on the AgNO$_3$ concentration, consistent with primary control of the AgNO$_3$ over aspect ratio occurring at the symmetry breaking point.

Advances in wet-chemistry techniques now enable the growth of a plethora of nanoparticle shapes and surface structures, opening a new realm of nanoparticle synthesis.[1–4] In part, this has been achieved by control of the rate of the crystal growth and/or surface selective passivation by surfactants and adsorbates.[3,5–7] The resulting novel anisotropic nanoparticle structures deviate greatly from those expected based on energy considerations.[2,3,5]

The Wulff construction, a powerful phenomenological theory, predicts nanocrystal shape by optimizing the balance between the nanocrystal surface energy and volume,[8,9] with constructions to incorporate twin planes and kinetic effects also reported.[10] In this approach, edge energies are a lower order energetic consideration provided the correct Gibbs equimolar partition for the surface is used.[6,11,12] In the limit of very small nanoparticles containing a higher fraction of coordinatively unsaturated atoms, a modified Gibbs-Thomson relationship with a non-linear size dependence better models experimental data.[13,14] This is consistent with the theoretical prediction that as a given facet reduces in size, the chemical potential goes towards infinity.[6] With this in mind, for particles with facets only a few atoms wide, the size and shape of the facets and proximity of facet intersections may have a significant influence.

Anisotropic structures are perhaps best exemplified by gold nanorods that exhibit both shape anisotropy and both high and low index surface faceting.[7,15,16] They can be synthesized with good control over the particle size,[17,18] morphology,[19,20] aspect ratio,[17,21] and tip structure.[19] Gold nanorods grown in the presence of silver nitrate and using ascorbic acid as reductant[17] are typically grown for

approximately 2 hours.[22,23] This growth time gives high yields of nanorods with aspect ratios that can be tuned from 2 to 4.5 as a function of the [HAuCl$_4$]:[AgNO$_3$] ratio.[17,23] However, at ~2 hours it has been shown that only ~15% of the gold precursor has been incorporated into the gold nanorods using this reductant.[22] Previous studies have shown that Au(I) ions can also be reduced to Au^0 by dehydroascorbic acid and 2,3-diketo-1-gulonic (oxidation products of ascorbic acid) and incorporated into the nanorods.[24–26] Therefore, gold nanorods grown for 2 hours do not represent the final product for this synthesis, but the nanorod structure at the point where rapid anisotropic growth has ceased and the growth has entered a much slower stage, controlled more by surface energy.[27,28]

As eluded to earlier, the side facets of gold nanorods have been observed as either low index ({0 0 1} and {0 1 1}) or high index ({0 1 1+√2} and the nearby {0 2 5}), as well as some mixing between the two.[7,15,16,29,30] This implies that the presence of surfactants, coupled with the mechanical constraints imposed by the overall geometry of the object, reduces the effective surface energy of the higher index facets.[7] The potential for continued gold nanorod growth beyond 2 hours raises the possibility that the variability in facets is due to the observation of gold nanorods at different growth times. Understanding which surface facets are present and when and how they evolve, and how their stability influences nanoparticle growth, remain important but outstanding challenges.

The gold nanorods here are synthesised by allowing the nanorods to remain in their original growth solution for periods up to 3 orders of magnitude longer than the conventional 2 hours. The extinction spectra of gold nanorods grown in the presence of 100 μM silver nitrate for up to 13 weeks are shown in Fig. 1a. Over this period, the wavelength of the longitudinal plasmon resonance blueshifts by 120 nm from 836 to 716 nm, suggesting a decrease in nanorod aspect ratio with time in agreement with previous reports.[26] A similar trend is observed for all silver nitrate concentrations (Fig. 1b). Fig. 1b and 1d show that the range of longitudinal LSPR wavelengths across the silver nitrate concentrations used narrows significantly, reducing from ~ 680 - 850 nm for rods grown for 2 hours to ~ 670 - 720 nm for rods grown for 13 weeks. As the longitudinal LSPR is directly dependent on nanorod aspect ratio over this range, these results show that all nanorods decrease in aspect ratio over time.
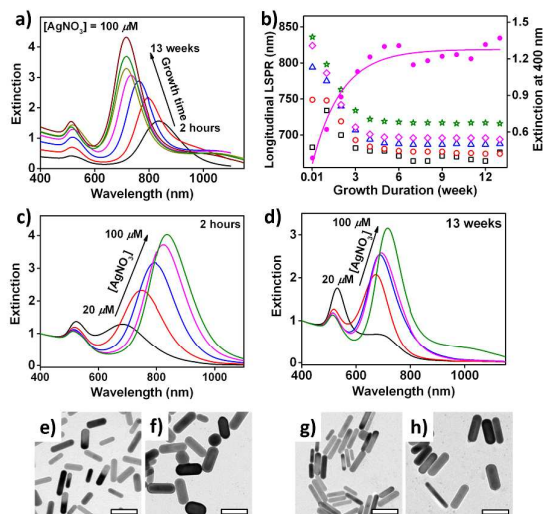
a. *ARC Centre of Excellence in Exciton Science, School of Chemistry, Monash University, Clayton, Victoria, 3800, Australia E-mail: alison.funston@monash.edu.*
b. *Department of Materials Science and Engineering, Monash University, Clayton, Victoria, 3800, Australia.*
c. *Monash Centre for Electron Microscopy and Department of Materials Science and Engineering, Monash University, Clayton, Victoria, 3800, Australia.*
† Electronic Supplementary Information (ESI) available. See DOI: 10.1039/x0xx00000x

The effect is greatest for nanorods with a larger initial aspect ratio, consequently the net effect is the aspect ratio converges to a smaller range. Also evident from the spectra in Fig. 1a is the increase in extinction at 400 nm, indicative of an increase in the concentration of metallic gold atoms.[31] The blue-shift and increase in extinction at 400 nm stabilize after 4-5 weeks (Fig. S1), indicating the blue-shift is predominantly associated with nanorod growth. The extinction at both the transverse and longitudinal LSPR wavelengths also increases. Therefore, the spectra suggest a significant increase in nanorod size over time, confirmed by TEM

Table 1. Average sizes, aspect ratios, and particle volumes of gold nanorods grown for 2 hours and 13 weeks as measured via TEM.

Ag μM	L_{2h} (nm)	L_{13w} (nm)	W_{2h} (nm)	W_{13w} (nm)	AR_{2h}	AR_{13w}	V_{2h} (×10^3 nm^3)	V_{13w} (×10^3 nm^3)
20	31(9)	40(11)	14(3)	20(6)	2.2 (0.8)	2.0 (0.8)	5(3)	12(7)
39	32(10)	45(9)	12(2)	19(4)	2.7 1.0)	2.4 (0.7)	3(2)	12(5)
59	32(10)	47(9)	11(2)	18(4)	2.9 (1.0)	2.6 (0.8)	3(2)	11(6)
80	38(10)	49(10)	11(2)	18(4)	3.5 (1.1)	2.7 (0.8)	4(2)	12(6)
100	40(9)	50(8)	10(2)	16(4)	4.0 (1.7)	3.1 (0.9)	3(2)	10(5)

a) The average volume is calculated assuming hemispherical tips and is the mean of the volumes of individual nanorods. b) Standard deviation shown in parenthesis. c) The numbers of particles analysed are reported in Table S1.

Fig. 1 (a) Extinction spectra of gold nanorods grown in 100 μM AgNO$_3$ for 2 hours (black), 1 (red), 2 (blue), 3 (magenta), 9 (dark yellow), 11 (olive), and 13 weeks (wine). (b) The change of longitudinal LSPR maxima during growth and change of extinction at 400 nm for gold nanorods grown in the presence of 80 μM AgNO$_3$ (pink dots, the line is a guide for the eye). The silver nitrate concentrations are 20 (black squares), 39 (red circles), 59 (blue triangles), 80 (pink diamonds), and 100 μM (olive stars). (c) and (d) Extinction spectra of gold nanorods grown for 2 hours and 13 weeks, respectively with AgNO$_3$ concentrations the same as (b). TEM images of gold nanorods grown in the presence of 39 μM AgNO$_3$ for (e) 2 hours and (f) 13 weeks and TEM images of gold nanorods grown in the presence of 100 μM AgNO$_3$ for (g) 2 hours and (h) 13 weeks (scale bars 50 nm).
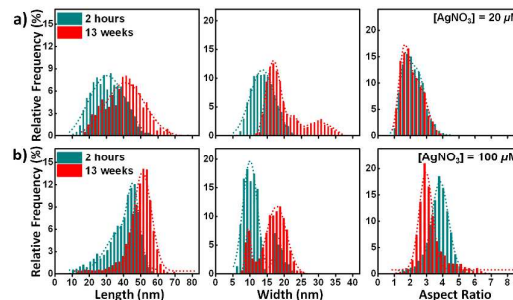
analysis (Fig. 1e - 1h, Fig. S2 and Table 1). Table 1 shows the particles increase significantly in length and width when grown from 2 hours to 13 weeks, resulting in a 2 - 3 fold increase in the average nanorod volume (Fig. S3). The larger growth percentage in width than length (Table 1) results in a decrease in aspect ratio and the observed blueshift of the longitudinal LSPR. This effect is greatest for nanorods grown in the presence of higher silver nitrate concentration (Fig. 2). The greater relative growth in width for the higher aspect ratio rods leads to a narrowing of aspect ratios (Table 1). Consequently, it may be concluded that the silver nitrate concentration does not influence the aspect ratio of the final product to the same degree as the product isolated at 2 hours.

To further understand the factors that drive shape control we utilise electron tomography[16,32–34] in an annular dark field scanning transmission electron microscopy (ADF-STEM) imaging mode to characterize the three-dimensional morphology of the nanorods and their surface facets. Fig. 3a and 3b show electron tomograms of nanorods grown in 80 μM AgNO$_3$ for 2 hours and 13 weeks. After separated by high index {0 1 1+√2} facets, in agreement with previous reports.[7] The nanorod surface also contains some undulations along the length of the rod (Movie S1 and S2). In

Fig. 2 Size distributions (length, width, and aspect ratio) of gold nanorods grown with (a) 39 and (b) 100 μM AgNO$_3$ for 2 hours (dark cyan) and 13 weeks (red). Dashed lines are Gaussian fits to the data. Table S1 lists the number of analysed particles.

comparison, after 13 weeks of growth the nanorod surfaces have become significantly smoother so that the cross-section of the nanorod is almost round. There is no obvious faceting in this structure, with the overall shape resembling a hemispherically capped cylinder. The surface free energy for rounded nanoparticle surfaces may be described using the weighted mean curvature (the ratio of the change in surface energy to the change in volume[6]), which leads to the definition of a weighted mean surface energy, $\bar{\gamma}$.

The nanorod morphology for a given growth time was further assessed using a quantitative analysis of ADF-STEM images, from which certain morphological features can be determined[33]. Fig. 3c and 3d show example ADF-STEM images of gold nanorods grown for 2 hours and 13 weeks, respectively. The gold nanorods grown for 2 hours contain atomically rough side surfaces, whereas those grown over 13 weeks have almost atomically smooth side surfaces (as highlighted by the intensity profiles). Furthermore, the "2 hours" rods have prominent {111} facets bridging the sides with the tips (as determined from the thickness profile in this region) but there are no clearly distinguishable facets detectable in the thickness profiles of the "13 weeks" rods. Collectively, these results show that, after a long growth period, there is growth in both width and length and a reduction in aspect ratio. Furthermore, the surface morphology evolves from a clearly faceted surface, with an alternating mix of high and low index side facets ({0 0 1}, {0 1 1+√2}, and {0 1 1}), to a smooth and round structure. These features are consistent across all particles for which ADF-STEM images on one or more zone axes were obtained > 30 particles (> 20 for the 2 hour sample and 10 for the 13 weeks). In the following, possible drivers of this shape change and implications for the mechanisms that govern shape control in gold nanorod synthesis are discussed.
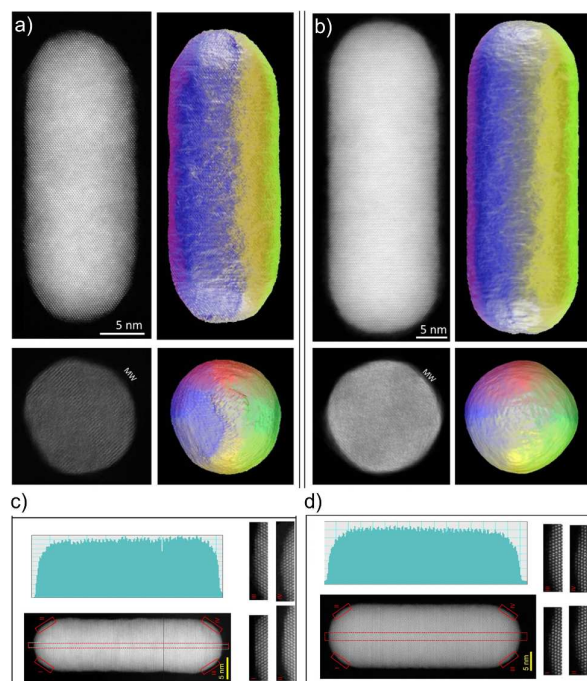
Fig. 3 ADF-STEM tomograms and corresponding cross sections for gold nanorods grown for (a) 2 hours and (b) 13 weeks in the presence of 80 μM AgNO$_3$. The left panel of each of these shows a single image from the tomographic tilt series (<011> orientation) and the right is the tomographic reconstruction along <011>. The bottom left panels show a cross-section slice taken from the middle of the rod's reconstruction while the right is the reconstruction viewed along the <001>. MW signifies the missing wedge. (c) and (d) are atomic resolution images of nanorods grown for (c) 2 hours and (d) 13 weeks with corresponding intensity line profiles integrated horizontally within the red rectangular region, highlighting the smoother surface along the length of the 13 week rod. Inserts I-IV show the bridging facets on each rod. The majority of the bridging facets for the 2 hour growth sample form {111} facets, whereas after 13 weeks there are no clearly distinguishable bridging facets.
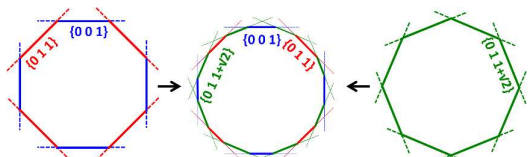
Fig. 4 Schematic showing observed[11, 12, 13, 27] combinations of of {0 0 1} (blue), {0 1 1+√2} (olive), and {0 1 1} (red) surface facets on gold nanorods and their geometric relationship.

Considering firstly the side facets, the nanorods grown using CTAB for 2 hours have been observed variously to exhibit high index facets,[15,16] close to {0 1 1+√2}, and low index facets {0 0 1} and {0 1 1},[29,30] or a mixture of all three that alternate in the sequence, {0 0 1}, {0 1 1+√2}, {0 1 1}, {0 1 1+√2}.[7] It is important to note here that the {0 1 1+√2} facet is defined by the plane that bisects the {0 0 1} and {0 1 1} planes, in other words, it truncates the vertex defined by the intersection of the {0 0 1} and {0 1 1} facets (Fig. 4) Although this indexing is irrational, we use it here to emphasise this point (the {0 1 1+√2} is very close in orientation to the reported {0 2 5}[15] or {0 5 12}[12, 13] side facets). As such, we hypothesize that the higher index facets emerge as surfaces that truncate the intersection between {0 0 1} and {0 1 1} facets (or possibly vice versa), as the nanorod cross-section evolves to become as round and smooth as possible to reduce the weighted mean curvature through the removal of high angle facet intersections and their associated energetically unfavourable edge atoms.[7,35] This is

supported by the significant rounding (or truncation) of the vertices observed previously for nanorods in which only one major family of facets is assigned.[11,12, 27] Given sufficient time, the logical outcome of a mechanism that favours the removal of edge atoms from small nanoscale (~ 2 nm) facets with very similar facet energies[7] is the eventual rounding of the overall surface structure. Additionally, the extended growth period studied here gives time for local surface restructuring that minimizes the overall surface energy by removing surface adatoms, steps and vacancies to create the atomically smooth structure observed after 13 weeks of growth. This process may be further facilitated by the preferential binding of surfactants (CTAB) and adsorbates (Ag$^+$) to more open surface sites, and an improved packing of the surfactant bilayer.[36,37]

A similar process at the nanorod tips would cause the observed transition from {111} facets to hemispherical tips. Importantly, if nanorod growth is driven in part by a surface selective passivation mechanism, the removal of {111} bridging facets represent the loss of the expected dominant site for gold deposition,[38,39] in favour of a higher index surface that may be passivated by a surfactant layer and/or adsorbates. As such, the observed change in surface faceting may be responsible for the transition from fast anisotropic growth to a much slower and more isotropic growth phase.

The process of thermodynamic energy minimization enabled by the long growth times reveals the thermodynamic stability of rounded surface structures under these growth conditions.[7,35] Underlying this is the role of surface mechanics in influencing the morphology of nanoscale objects, where the facets are only a few atoms wide and the surface chemical potential is increased (relative to larger facets). Intertwined with these factors is the predilection of surface additives, such as those here, to stabilize atomically open surfaces. This combination of mechanical forces coupled with surfactant chemistry defines the final surface morphology.

It is energetically favourable to minimize facet intersections and remove highly-energetic corner and edge atoms[35] and, in the longer term, this drives the evolution of the nanorod morphology to a final, smooth and round product. In this final nanorod product, rounding of all surface facets removes the crystallographic distinction between the surfaces present, creating instead a seemingly isotropic weighted mean curvature. At this point, surface energetics is no longer influenced by specific facet crystallography but is now driven by a need to reduce the overall surface to volume ratio by reducing the aspect ratio of the nanorod. However, whilst all nanorods reduce in aspect ratio, after approximately 6 weeks each rod sample reaches a stable shape, and maintains this aspect ratio during further growth (Figure 1b).

The final rounded nanorod morphology represents a hemispherically capped cylinder with approximately homogenous surfaces. We hypothesize that the stability of the final nanorod aspect ratio represents the local minimum energy structure driven by the specific weighted mean curvature of the nanoparticle. The anisotropic shape is preserved due to differences in curvature on the side of the nanorods relative to the tips. Two weighted mean surface curvatures can be defined, the cylindrical curvature at the sides and the spherical curvature at the tips. The difference between these can be expected to result in an intrinsic energetic differentiation due to a difference in their relative surface tension terms, as well as cause an inhomogeneous packing of the surfactant

bilayer across the particle,[20,40] with both effects contributing to give different effective chemical potentials for the side and tips at the surfactant-solution interface. Monte-Carlo simulations predict the nanorods converge to a given aspect ratio dependent upon the S_{side} : S_{tip} surface energy terms,[28] consistent with our experimental results here and for overgrowth of nanorods in an equilibrated system.[41] Furthermore, it is notable that whilst all nanorods reduce in aspect ratio towards a common value, some dependency remains on the initial silver nitrate concentration. This is indicative of some difference in surface energetics between the samples. Differences in the initial nanorod widths as a function of silver nitrate concentration would lead to small changes in the final weighted mean curvature terms, thereby explaining the difference in the final nanorod aspect ratios.

In conclusion, gold nanorods are allowed to grow continuously for a period 1000 times longer than for the usual synthesis (13 weeks). The evolution of size, shape, structure, and surface morphology during this period as a function of silver nitrate concentration is described. A shift of the longitudinal localized surface plasmon resonant wavelength occurs over time for all silver nitrate concentrations, corresponding to a reduction in gold nanorod aspect ratios. All nanorods grow in both width and length, with a greater percentage growth in width. This leads to an overall reduction in aspect ratio. Moreover, this growth phase is more prominent in the higher aspect ratio rods, causing a narrowing and convergence of the range of aspect ratios to ~ 2 - 3. This shows a reduction in the control exerted by silver nitrate on the aspect ratio over longer timeframes. The surface morphology of gold nanorods experiences a transition from a clearly faceted surface to a round and atomically smooth surface over time, influencing the final aspect ratio of the nanorods.

Conflicts of interest

There are no conflicts to declare.

Notes and references

1 M. Grzelczak, J. Pérez-Juste, P. Mulvaney and L. M. Liz-Marzán, *Chem. Soc. Rev.*, 2008, **37**, 1783.
2 M. L. Personick, M. R. Langille, J. Zhang and C. A. Mirkin, *Nano Lett.*, 2011, **11**, 3394–3398.
3 M. L. Personick and C. A. Mirkin, *J. Am. Chem. Soc.*, 2013, **135**, 18238–18247.
4 Y. Xia, X. Xia and H.-C. Peng, *J. Am. Chem. Soc.*, 2015, **137**, 7947–7966.
5 M. R. Langille, M. L. Personick, J. Zhang and C. A. Mirkin, *J. Am. Chem. Soc.*, 2012, **134**, 14542–14554.
6 L. D. Marks and L. Peng, *J. Phys. Condens. Matter*, 2016, **28**, 53001.
7 H. Katz-Boon, M. Walsh, C. Dwyer, P. Mulvaney, A. M. Funston and J. Etheridge, *Nano Lett.*, 2015, **15**, 1635–1641.
8 Wulff, George, *Z. Kryst. Mineral.*, 1901, **34**, 449–530.
9 L. D. Marks, *Rep. Prog. Phys.*, 1994, **57**, 603–649.
10 E. Ringe, R. P. Van Duyne and L. D. Marks, *J. Phys. Chem. C*, 2013, **117**, 15859–15870.
11 C. L. Cleveland and U. Landman, *J. Chem. Phys.*, 1991, **94**, 7376–7396.
12 J. C. Hamilton, *Phys. Rev. B*, 2006, **73**, 125447.
13 S. C. Parker and C. T. Campbell, *Phys. Rev. B*, 2007, **75**, 35430.
14 C. T. Campbell, *Science*, 2002, **298**, 811–814.
15 E. Carbó-Argibay, B. Rodríguez-González, S. Gómez-Graña, A. Guerrero-Martínez, I. Pastoriza-Santos, J. Pérez-Juste and L. M. Liz-Marzán, *Angew. Chem. Int. Ed.*, 2010, **49**, 9397–9400.
16 H. Katz-Boon, C. J. Rossouw, M. Weyland, A. M. Funston, P. Mulvaney and J. Etheridge, *Nano Lett.*, 2011, **11**, 273–278.
17 B. Nikoobakht and M. A. El-Sayed, *Chem. Mater.*, 2003, **15**, 1957–1962.
18 T. K. Sau and C. J. Murphy, *Langmuir*, 2004, **20**, 6414–6420.
19 X. Ye, Y. Gao, J. Chen, D. C. Reifsnyder, C. Zheng and C. B. Murray, *Nano Lett.*, 2013, **13**, 2163–2171.
20 J. Pérez-Juste, L. M. Liz-Marzán, S. Carnie, D. Y. C. Chan and P. Mulvaney, *Adv. Funct. Mater.*, 2004, **14**, 571–579.
21 L. Zhang, K. Xia, Z. Lu, G. Li, J. Chen, Y. Deng, S. Li, F. Zhou and N. He, *Chem. Mater.*, 2014, **26**, 1794–1798.
22 C. J. Orendorff and C. J. Murphy, *J. Phys. Chem. B*, 2006, **110**, 3990–3994.
23 W. Tong, M. J. Walsh, P. Mulvaney, J. Etheridge and A. M. Funston, *J. Phys. Chem. C*, 2017, **121**, 3549–3559.
24 L. Gou and C. J. Murphy, *Chem. Mater.*, 2005, **17**, 3668–3672.
25 N. D. Burrows, S. Harvey, F. A. Idesis and C. J. Murphy, *Langmuir*, 2017, **33**, 1891–1907.
26 C. L. John, S. L. Strating, K. A. Shephard and J. X. Zhao, *RSC Adv.*, 2013, **3**, 10909.
27 K. Park, L. F. Drummy, R. C. Wadams, H. Koerner, D. Nepal, L. Fabris and R. A. Vaia, *Chem. Mater.*, 2013, **25**, 555–563.
28 J. A. Edgar, A. M. McDonagh and M. B. Cortie, *ACS Nano*, 2012, **6**, 1116–1125.
29 Z. L. Wang, M. B. Mohamed, S. Link and M. A. El-Sayed, *Surf. Sci.*, 1999, **440**, L809–L814.
30 B. Goris, S. Bals, W. Van den Broek, E. Carbó-Argibay, S. Gómez-Graña, L. M. Liz-Marzán and G. Van Tendeloo, *Nat. Mater.*, 2012, **11**, 930–935.
31 L. Scarabelli, A. Sánchez-Iglesias, J. Pérez-Juste and L. M. Liz-Marzán, *J. Phys. Chem. Lett.*, 2015, **6**, 4270–4279.
32 P. A. Midgley and M. Weyland, *Ultramicroscopy*, 2003, **96**, 413–431.
33 H. Katz-Boon, C. J. Rossouw, C. Dwyer and J. Etheridge, *Ultramicroscopy*, 2013, **124**, 61–70.
34 C. J. Rossouw, C. Dwyer, H. Katz-Boon and J. Etheridge, *Ultramicroscopy*, 2014, **136**, 216–223.
35 D. Alpay, L. Peng and L. D. Marks, *J. Phys. Chem. C*, 2015, **119**, 21018–21023.
36 G. Grochola, I. K. Snook and S. P. Russo, *J. Chem. Phys.*, 2007, **127**, 194707.
37 N. Almora-Barrios, G. Novell-Leruth, P. Whiting, L. M. Liz-Marzán and N. López, *Nano Lett.*, 2014, **14**, 871–875.
38 M. J. Walsh, S. J. Barrow, W. Tong, A. M. Funston and J. Etheridge, *ACS Nano*, 2015, **9**, 715–724.
39 Liu, M. Z. and P. Guyot-Sionnest, *J. Phys. Chem. B*, 2005, **109**, 22192–22200.
40 B. Nikoobakht and M. A. El-Sayed, *Langmuir*, 2001, **17**, 6368–6374.
41 L. Scarabelli, M. Grzelczak and L. M. Liz-Marzán, *Chem. Mater.*, 2013, **25**, 4232–4238.